10
Input Filter Design

10.1 INTRODUCTION

10.1.1 Conducted EMI

It is nearly always required that a filter be added at the power input of a switching converter. By attenuating the switching harmonics that are present in the converter input current waveform, the input filter allows compliance with regulations that limit *conducted electromagnetic interference* (EMI). The input filter can also protect the converter and its load from transients that appear in the input voltage $v_g(t)$, thereby improving the system reliability.

A simple buck converter example is illustrated in Fig. 10.1. The converter injects the pulsating current $i_g(t)$ of Fig. 10.1(b) into the power source $v_g(t)$. The Fourier series of $i_g(t)$ contains harmonics at multiples of the switching frequency f_s, as follows:

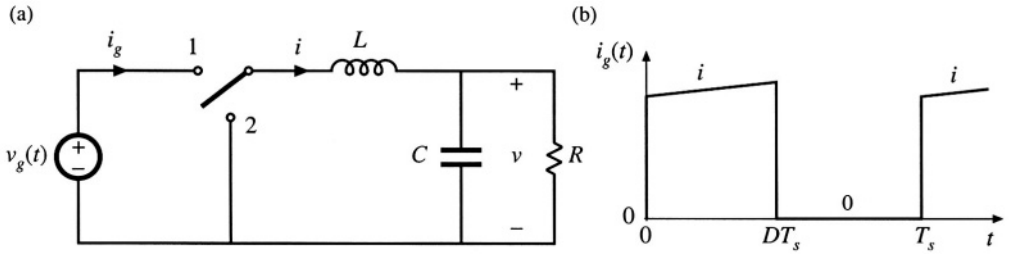

Fig. 10.1 Buck converter example: (a) circuit of power stage, (b) pulsating input current waveform.

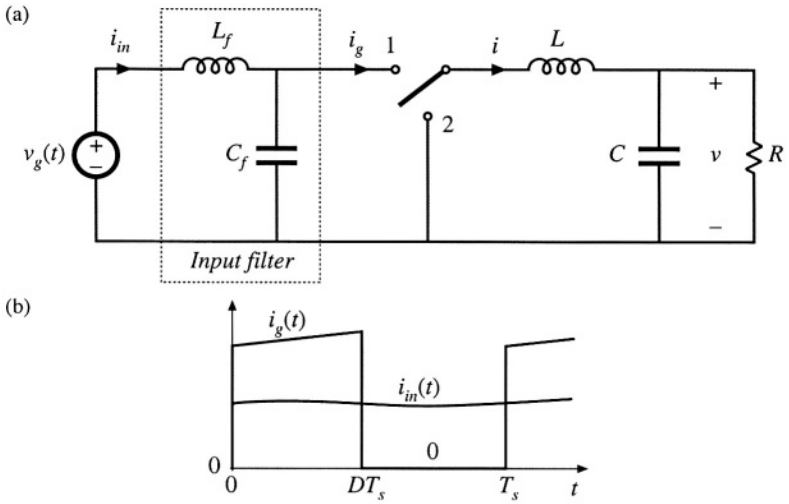

Fig. 10.2 Addition of a simple *L-C* low-pass filter to the power input terminals of the buck converter: (a) circuit. (b) input current waveforms.

$$i_g(t) = DI + \sum_{k=1}^{\infty} \frac{2I}{k\pi} \sin\left(k\pi D\right) \cos\left(k\omega t\right) \tag{10.1}$$

In practice, the magnitudes of the higher-order harmonics can also be significantly affected by the current spike caused by diode reverse recovery, and also by the finite slopes of the switching transitions. The large high-frequency current harmonics of $i_g(t)$ can interfere with television and radio reception, and can disrupt the operation of nearby electronic equipment. In consequence, regulations and standards exist that limit the amplitudes of the harmonic currents injected by a switching converter into its power source [1-8]. As an example, if the dc inductor current i of Fig. 10.2 has a magnitude of several Amperes, then the fundamental component ($n = 1$) has an rms amplitude in the vicinity of one Ampere. Regulations may require attenuation of this current to a value typically in the range 10 μA to 100 μA.

To meet limits on conducted EMI, it is necessary to add an input filter to the converter. Figure 10.2 illustrates a simple single-section *L-C* low-pass filter, added to the input of the converter of Fig. 10.1. This filter attenuates the current harmonics produced by the switching converter, and thereby smooths the current waveform drawn from the power source. If the filter has transfer function $H(s) = i_{in}/i_g$, then the input current Fourier series becomes

$$i_{in}(t) = H(0)DI + \sum_{k=1}^{\infty} \left\| H(kj\omega) \right\| \frac{2I}{k\pi} \sin\left(k\pi D\right) \cos\left(k\omega t + \angle H(kj\omega)\right) \tag{10.2}$$

In other words, the amplitude of each current harmonic at angular frequency $k\omega$ is attenuated by the filter transfer function at the harmonic frequency, $\| H(kj\omega) \|$. Typical requirements effectively limit the current harmonics to have amplitudes less than 100 μA, and hence input filters are often required to attenuate the current amplitudes by 80 dB or more.

To improve the reliability of the system, input filters are sometimes required to operate normally when transients or periodic disturbances are applied to the power input. Such *conducted susceptibility* specifications force the designer to damp the input filter resonances, so that input disturbances do not excite excessive currents or voltages within the filter or converter.

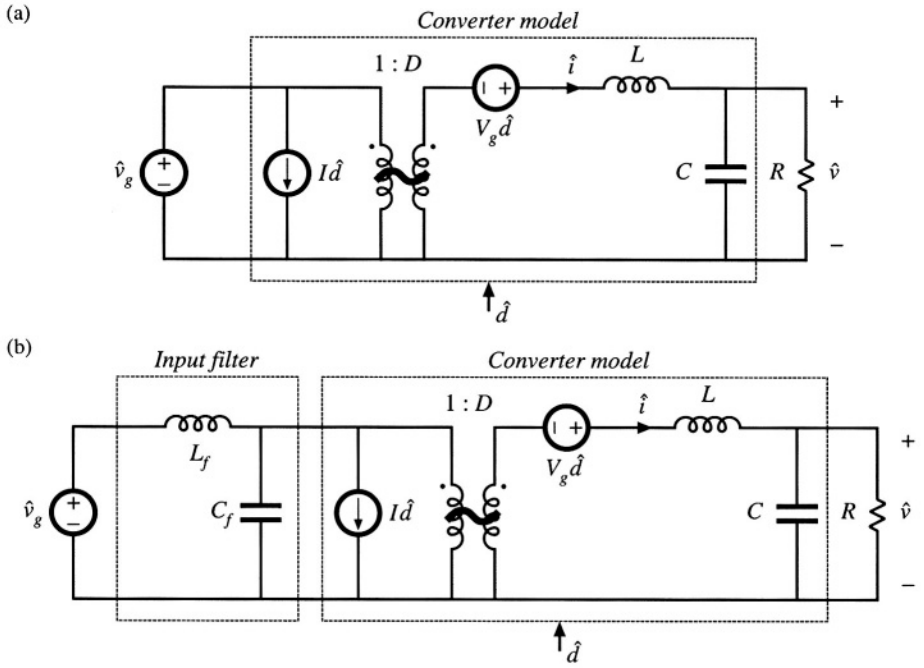

Fig. 10.3 Small-signal equivalent circuit models of the buck converter: (a) basic converter model, (b) with addition of input filter.

10.1.2 The Input Filter Design Problem

The situation faced by the design engineer is typically as follows. A switching regulator has been designed, which meets performance specifications. The regulator was properly designed as discussed in Chapter 9, using a small-signal model of the converter power stage such as the equivalent circuit of Fig. 10.3(a). In consequence, the transient response is well damped and sufficiently fast, with adequate phase margin at all expected operating points. The output impedance is sufficiently small over a wide frequency range. The line-to-output transfer function $G_{vg}(s)$, or *audiosusceptibility,* is sufficiently small, so that the output voltage remains regulated in spite of variations in $\hat{v}_g(t)$.

Having developed a good design that meets the above goals regarding dynamic response, the problem of conducted EMI is then addressed. A low-pass filter having attenuation sufficient to meet conducted EMI specifications is constructed and added to the converter input. A new problem then arises: the input filter changes the dynamics of the converter. The transient response is modified, and the control system may even become unstable. The output impedance may become large over some frequency range, possibly exhibiting resonances. The audiosusceptibility may be degraded.

The problem is that the input filter affects the dynamics of the converter, often in a manner that degrades regulator performance. For example, when a single-section *L-C* input filter is added to a buck converter as in Fig. 10.2(a), the small-signal equivalent circuit model is modified as shown in Fig. 10.3(b). The input filter elements affect all transfer functions of the converter, including the control-to-

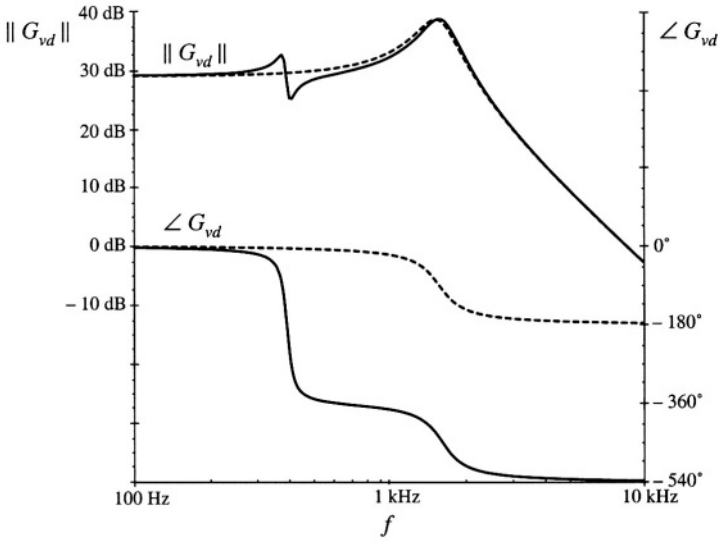

Fig. 10.4 Control-to-output transfer functions predicted by the equivalent circuit models of Fig. 10.3. *Dashed lines:* without input filter [Fig. 10.3(a)]. *Solid lines:* with input filter [Fig. 10.3(b)].

output transfer function $G_{vg}(s)$, the line-to-output transfer function $G_{vg}(s)$, and the converter output impedance $Z_{out}(s)$. Moreover, the influence of the input filter on these transfer functions can be quite severe.

As an illustration, let's examine how the control-to-output transfer function $G_{vd}(s)$ of the buck converter of Fig. 10.1 is altered when a simple *L-C* input filter is added as in Fig. 10.2. For this example, the element values are chosen to be: $D = 0.5$, $L = 100\ \mu H$, $C = 100\ \mu F$, $R = 3\ \Omega$, $L_f = 330\ \mu H$, $C_f = 470\ \mu F$. Figure 10.4 contains the Bode plot of the magnitude and phase of the control-to-output transfer function $G_{vd}(s)$. The dashed lines are the magnitude and phase before the input filter was added, generated by solution of the model of Fig. 10.3(a). The complex poles of the converter output filter cause the phase to approach – 180° at high frequency. Usually, this is the model used to design the regulator feedabck loop and to evaluate the phase margin (*see* Chapter 9). The solid lines of Fig. 10.4 show the magnitude and phase after addition of the input filter, generated by solution of the model of Fig. 10.3(b). The magnitude exhibits a "glitch" at the resonant frequency of the input filter, and an additional - 360° of phase shift is introduced into the phase. It can be shown that $G_{vd}(s)$ now contains an additional complex pole pair and a complex right half-plane zero pair, associated with the input filter dynamics. If the crossover frequency of the regulator feedback loop is near to or greater than the resonant frequency of the input filter, then the loop phase margin will become negative and instability will result. Such behavior is typical; consequently, input filters are notorious for destabilizing switching regulator systems.

This chapter shows how to mitigate the stability problem, by introducing damping into the input filter and by designing the input filter such that its output impedance is sufficiently small [9-21]. The result of these measures is that the effect of the input filter on the control-to-output transfer function becomes negligible, and hence the converter dynamics are much better behaved. Although analysis of the fourth-order system of Fig. 10.3(b) is potentially quite complex, the approach used here simplifies the problem through use of impedance inequalities involving the converter input impedance and the filter output impedance [9,10]. These inequalities are based on Middlebrook's extra element theorem of Appendix C. This approach allows the engineer to gain the insight needed to effectively design the input filter. Optimization of the damping networks of input filters, and design of multiple-section filters, is also discussed.

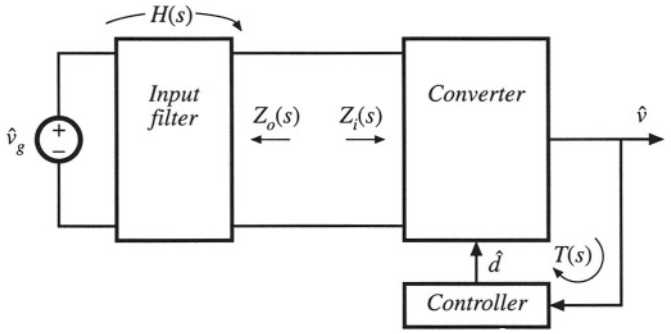

Fig. 10.5 Addition of an input filter to a switching voltage regulator system.

10.2 EFFECT OF AN INPUT FILTER ON CONVERTER TRANSFER FUNCTIONS

The control-to-output transfer function $G_{vd}(s)$ is defined as follows:

$$G_{vd}(s) = \left.\frac{\hat{v}(s)}{\hat{d}(s)}\right|_{\hat{v}_g(s)=0} \tag{10.3}$$

The control-to-output transfer functions of basic CCM converters with no input filters are listed in Section 8.2.2.

Addition of an input filter to a switching regulator leads to the system illustrated in Fig. 10.5. To determine the control-to-output transfer function in the presence of the input filter, we set $\hat{v}_g(s)$ to zero and solve for $\hat{v}(s)/\hat{d}(s)$ according to Eq. (10.3). The input filter can then be represented simply by its output impedance $Z_o(s)$ as illustrated in Fig. 10.6. Thus, the input filter can be treated as an extra element having impedance $Z_o(s)$. In Appendix C, Section C.4.3, Middlebrook's extra element theorem is employed to determine how addition of the input filter modifies the control-to-output transfer function. It is found that the modified control-to-output transfer function can be expressed as follows [9]:

$$G_{vd}(s) = \left(G_{vd}(s)\Big|_{Z_o(s)=0} \right) \frac{\left(1 + \frac{Z_o(s)}{Z_N(s)}\right)}{\left(1 + \frac{Z_o(s)}{Z_D(s)}\right)} \tag{10.4}$$

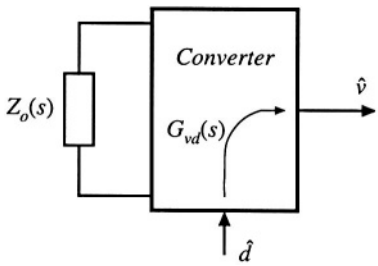

Fig. 10.6 Determination of the control-to-output transfer function $G_{vd}(s)$ for the system of Fig. 10.5.

Table 10.1 Input filter design criteria for basic converters

Converter	$Z_N(s)$	$Z_D(s)$	$Z_e(s)$
Buck	$-\frac{R}{D^2}$	$\frac{R}{D^2}\frac{\left(1+s\frac{L}{R}+s^2LC\right)}{\left(1+sRC\right)}$	$\frac{sL}{D^2}$
Boost	$-D'^2R\left(1-\frac{sL}{D'^2R}\right)$	$D'^2R\frac{\left(1+s\frac{L}{D'^2R}+s^2\frac{LC}{D'^2}\right)}{\left(1+sRC\right)}$	sL
Buck–boost	$-\frac{D'^2R}{D^2}\left(1-\frac{sDL}{D'^2R}\right)$	$\frac{D'^2R}{D^2}\frac{\left(1+s\frac{L}{D'^2R}+s^2\frac{LC}{D'^2}\right)}{\left(1+sRC\right)}$	$\frac{sL}{D^2}$

where

$$G_{vd}(s)\Big|_{Z_o(s)=0} \tag{10.5}$$

is the original control-to-output transfer function with no input filter. The quantity $Z_D(s)$ is equal to the converter input impedance $Z_i(s)$ under the condition that $\hat{d}(s)$ is equal to zero:

$$Z_D(s) = Z_i(s)\Big|_{d(s)=0} \tag{10.6}$$

The quantity $Z_N(s)$ is equal to the converter input impedance $Z_i(s)$ under the condition that the feedback controller of Fig. 10.5 operates ideally; in other words, the controller varies $\hat{d}(s)$ as necessary to maintain $\hat{v}(s)$ equal to zero:

$$Z_N(s) = Z_i(s)\Big|_{v(s)\rightarrow 0} \tag{10.7}$$

In terms of the canonical circuit model parameters described in Section 7.5, $Z_N(s)$ can be shown to be

$$Z_N(s) = -\frac{e(s)}{j(s)} \tag{10.8}$$

Expressions for $Z_N(s)$ and $Z_D(s)$ for the basic buck, boost, and buck-boost converters are listed in Table 10.1.

10.2.1 Discussion

Equation (10.4) relates the power stage control-to-output transfer function $G_{vd}(s)$ to the output impedance $Z_o(s)$ of the input filter, and also to the quantities $Z_N(s)$ and $Z_D(s)$ measured at the power input port of the converter. The quantity $Z_D(s)$ coincides with the open-loop input impedance of the converter.

As described above, the quantity $Z_N(s)$ is equal to the input port impedance of the converter

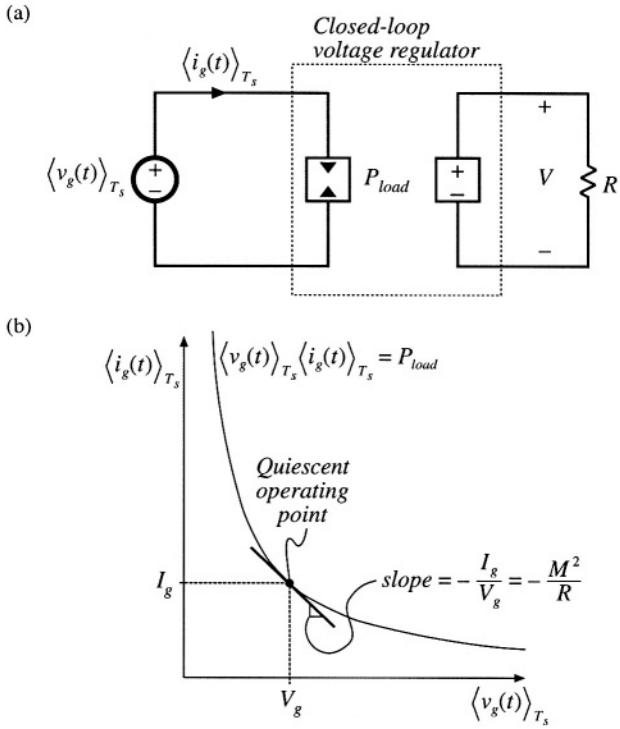

Fig. 10.7 Power input port characteristics of an ideal switching voltage regulator: (a) equivalent circuit model, including dependent power sink, (b) constant power characteristic of input port.

power stage, under the conditions that $\hat{d}(s)$ is varied as necessary to null $\hat{v}(s)$ to zero. This is, in fact, the function performed by an ideal controller: it varies the duty cycle as necessary to maintain zero error of the output voltage. Therefore, $Z_N(s)$ coincides with the impedance that would be measured at the converter power input terminals, if an ideal feedback loop perfectly regulated the converter output voltage. Of course, Eq. (10.4) is valid in general, regardless of whether a control system is present.

Figure 10.7 illustrates the large-signal behavior of a feedback loop that perfectly regulates the converter output voltage. Regardless of the applied input voltage $v_g(t)$, the output voltage is maintained equal to the desired value V. The load power is therefore constant, and equal to $P_{load} = V^2/R$. In the idealized case of a lossless converter, the power flowing into the converter input terminals will also be equal to P_{load}, regardless of the value of $v_g(t)$. Hence, the power input terminal of the converter obeys the equation

$$\langle v_g(t) \rangle_{T_s} \langle i_g(t) \rangle_{T_s} = P_{load} \tag{10.9}$$

This characteristic is illustrated in Fig. 10.7(b), and is represented in Fig. 10.7(a) by the dependent power sink symbol. The properties of power sources and power sinks are discussed in detail in Chapter 11.

Figure 10.7(b) also illustrates linearization of the constant input power characteristic, about a quiescent operating point. The resulting line has negative slope; therefore, the incremental (small signal) input resistance of the ideal voltage regulator is negative. For example, increasing the voltage $\langle v_g(t) \rangle_{T_s}$

causes the current $\langle i_g(t) \rangle_{T_s}$ to decrease, such that the power remains constant. This incremental resistance has the value [9,14]:

$$-\frac{R}{M^2} \tag{10.10}$$

where R is the output load resistance, and M is the conversion ratio V/V_g. For each of the converters listed in Table 10.1, the dc asymptote of $Z_N(s)$ coincides with the negative incremental resistance given by the equation above.

Practical control systems exhibit a limited bandwidth, determined by the crossover frequency f_c of the feedback loop. Therefore, we would expect the closed-loop regulator input impedance to be approximately equal to $Z_N(s)$ at low frequency ($f \ll f_c$) where the loop gain is large and the regulator works well. At frequencies above the bandwidth of the regulator ($f \gg f_c$), we expect the converter input impedance to follow the open-loop value $Z_D(s)$. For closed-loop conditions, it can be shown that the regulator input impedance $Z_i(s)$ is, in fact, described by the following equation:

$$\frac{1}{Z_i(s)} = \frac{1}{Z_N(s)} \frac{T(s)}{1+T(s)} + \frac{1}{Z_D(s)} \frac{1}{1+T(s)} \tag{10.11}$$

where $T(s)$ is the controller loop gain. Thus, the regulator input impedance follows the negative resistance of $Z_N(s)$ at low frequency where the magnitude of the loop gain is large [and hence $T/(1+T) \approx 1$, $1/(1+T) \approx 0$], and reverts to the (positive) open-loop impedance $Z_D(s)$ at high frequency where $\| T \|$ is small [i.e., where $T/(1+T) \approx 0$, $1/(1+T) \approx 1$].

When an undamped or lightly damped input filter is connected to the regulator input port, the input filter can interact with the negative resistance characteristic of Z_N to form a *negative resistance oscillator*. This further explains why addition of an input filter tends to lead to instabilities.

10.2.2 Impedance Inequalities

Equation (10.4) reveals that addition of the input filter causes the control-to-output transfer function to be modified by the factor

$$\frac{\left(1 + \frac{Z_o(s)}{Z_N(s)}\right)}{\left(1 + \frac{Z_o(s)}{Z_D(s)}\right)} \tag{10.12}$$

called the *correction factor*. When the following inequalities are satisfied,

$$\begin{aligned} \left| Z_o \right| &\ll \left| Z_N \right|, \text{ and} \\ \left| Z_o \right| &\ll \left| Z_D \right| \end{aligned} \tag{10.13}$$

then the correction factor has a magnitude of approximately unity, and the input filter does not substantially alter the control-to-output transfer function [9,10]. These inequalities limit the maximum allowable output impedance of the input filter, and constitute useful filter design criteria. One can sketch the Bode plots of $\| Z_N(j\omega) \|$ and $\| Z_D(j\omega) \|$, and compare with the Bode plot of $\| Z_o(j\omega) \|$. This allows the engineer to gain the insight necessary to design an input filter that satisfies Eq. (10.13).

A similar analysis shows that the converter output impedance is not substantially affected by the input filter when the following inequalities are satisfied:

$$\begin{aligned} |Z_o| &\ll |Z_e|, \text{ and} \\ |Z_o| &\ll |Z_D| \end{aligned} \tag{10.14}$$

where $Z_D(s)$ is again as given in Table 10.1. The quantity $Z_e(s)$ is equal to the converter input impedance $Z_i(s)$ under the conditions that the converter output is shorted:

$$Z_e = Z_i\big|_{\hat{v}_g = 0} \tag{10.15}$$

Expressions for $Z_e(s)$ for basic converters are also listed in Table 10.1.

Similar impedance inequalities can be derived for the case of current-programmed converters [12,13], or converters operating in the discontinuous conduction mode. In [12], impedance inequalities nearly identical to the above equations were shown to guarantee that the input filter does not degrade transient response and stability in the current-programmed case. Feedforward of the converter input voltage was suggested in [16].

10.3 BUCK CONVERTER EXAMPLE

Let us again consider the example of a simple buck converter with *L-C* input filter, as illustrated in Fig. 10.8(a). Upon replacing the converter with its small-signal model, we obtain the equivalent circuit of Fig. 10.8(b). Let's evaluate Eq. (10.4) for this example, to find how the input filter modifies the control-to-output transfer function of the converter.

10.3.1 Effect of Undamped Input Filter

The quantities $Z_N(s)$ and $Z_D(s)$ can be read from Table 10.1, or can be derived using Eqs. (10.6) and (10.7) as further described in Appendix C. The quantity $Z_D(s)$ is given by Eq. (10.6). Upon setting $\hat{d}(s)$ to zero, the converter small signal model reduces to the circuit of Fig. 10.9(a). It can be seen that $Z_D(s)$ is equal to the input impedance of the *R-L-C* filter, divided by the square of the turns ratio:

$$Z_D(s) = \frac{1}{D^2}\left(sL + R \| \frac{1}{sC}\right) \tag{10.16}$$

Construction of asymptotes for this impedance is treated in Section 8.4, with the results for the numerical values of this example given in Fig. 10.10. The load resistance dominates the impedance at low frequency, leading to a dc asymptote of $R/D^2 = 12\ \Omega$. For the high-Q case shown, $\| Z_D(j\omega) \|$ follows the output capacitor asymptote, reflected through the square of the effective turns ratio, at intermediate frequencies. A series resonance occurs at the output filter resonant frequency f_0, given by

$$f_0 = \frac{1}{2\pi\sqrt{LC}} \tag{10.17}$$

For the element values listed in Fig. 10.8(a), the resonant frequency is $f_0 = 1.6$ kHz. The values of the asymptotes at the resonant frequency f_0 are given by the characteristic impedance R_0, referred to the

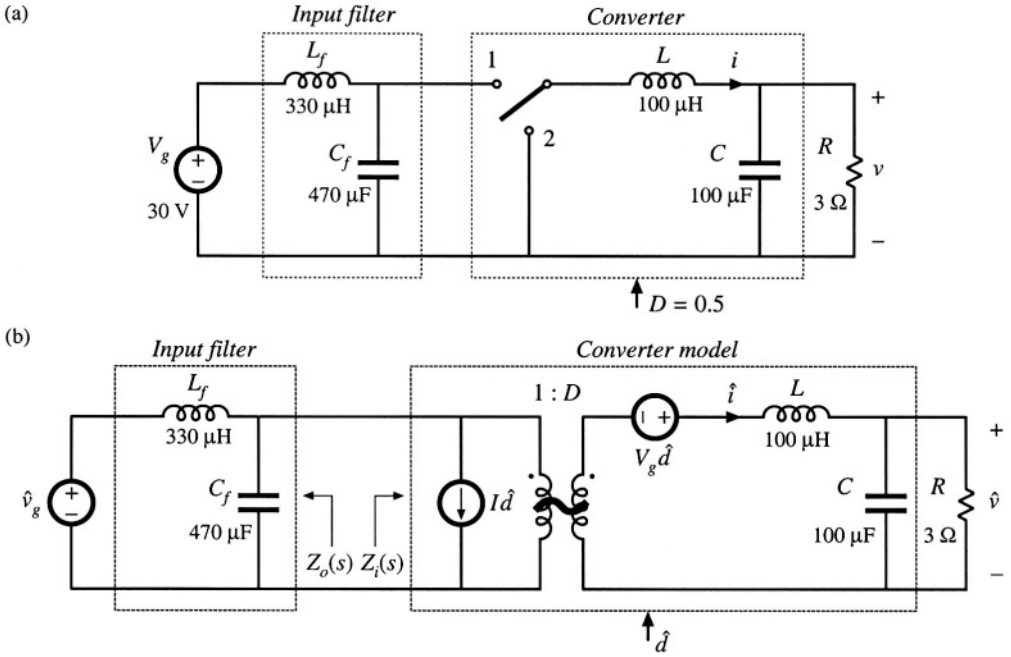

Fig. 10.8 Buck converter example: (a) converter circuit, (b) small-signal model.

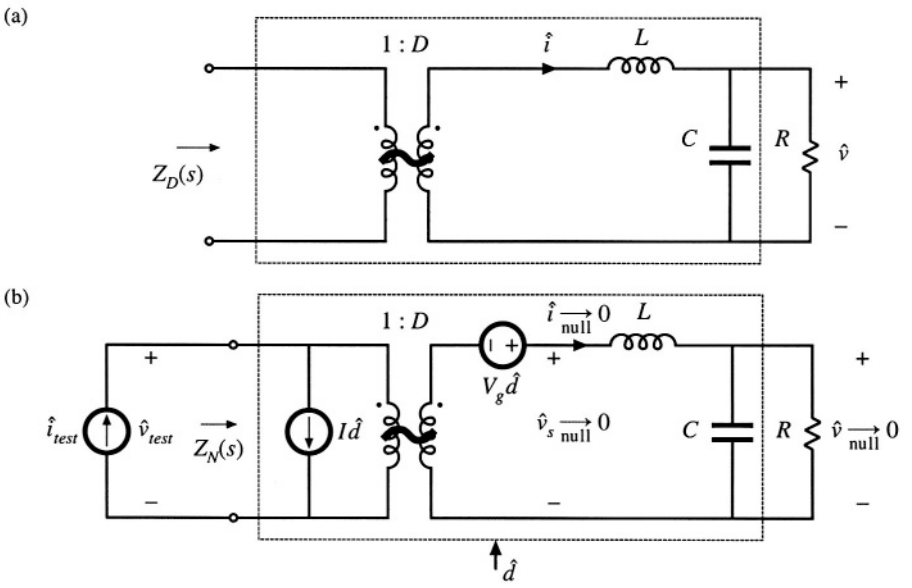

Fig. 10.9 Determination of the quantities $Z_N(s)$ and $Z_D(s)$ for the circuit of Fig. 10.8(b): (a) determination of $Z_D(s)$, (b) determination of $Z_N(s)$.

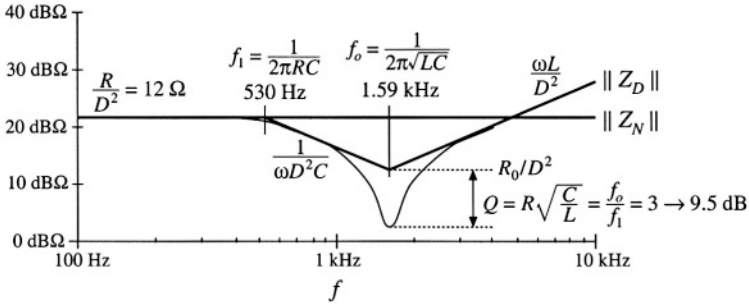

Fig. 10.10 Construction of $\| Z_N(j\omega) \|$ and $\| Z_D(j\omega) \|$, buck converter example.

transformer primary:

$$\frac{R_0}{D^2} = \frac{1}{D^2}\sqrt{\frac{L}{C}} \tag{10.18}$$

For the element values given in Fig. 10.8(a), this expression is equal to 4 Ω. The Q-factor is given by

$$Q = \frac{R}{R_0} = R\sqrt{\frac{C}{L}} \tag{10.19}$$

This expression yields a numerical value of $Q = 3$. The value of $\| Z_D(j\omega) \|$ at the resonant frequency 1.6 kHz is therefore equal to (4 Ω)/(3) = 1.33 Ω. At high frequency, $\| Z_D(j\omega) \|$ follows the reflected inductor asymptote.

The quantity $Z_N(s)$ is given by Eq. (10.7). This impedance is equal to the converter input impedance $Z_i(s)$, under the conditions that $\hat{d}(s)$ is varied to maintain the output voltage $\hat{v}(s)$ at zero. Figure 10.9(b) illustrates the derivation of an expression for $Z_N(s)$. A test current source $\hat{i}_{test}(s)$ is injected at the converter input port. The impedance $Z_N(s)$ can be viewed as the transfer function from $\hat{i}_{test}(s)$ to $\hat{v}_{test}(s)$:

$$Z_N(s) = \left.\frac{\hat{v}_{test}(s)}{\hat{i}_{test}(s)}\right|_{\hat{v} \xrightarrow[null]{} 0} \tag{10.20}$$

The null condition $\hat{v}(s) \xrightarrow[null]{} 0$ greatly simplifies analysis of the circuit of Fig. 10.9(b). Since the voltage $\hat{v}(s)$ is zero, the currents through the capacitor and load impedances are also zero. This further implies that the inductor current $\hat{i}(s)$ and transformer winding currents are zero, and hence the voltage across the inductor is also zero. Finally, the voltage $\hat{v}_s(s)$, equal to the output voltage plus the inductor voltage, is zero.

Since the currents in the windings of the transformer model are zero, the current $i_{test}(s)$ is equal to the independent source current $I\hat{d}(s)$:

$$\hat{i}_{test}(s) = I\hat{d}(s) \tag{10.21}$$

Because $\hat{v}_s(s)$ is equal to zero, the voltage applied to the secondary of the transformer model is equal to the independent source voltage $-V_g\hat{d}(s)$. Upon dividing by the turns ratio D, we obtain $\hat{v}_{test}(s)$:

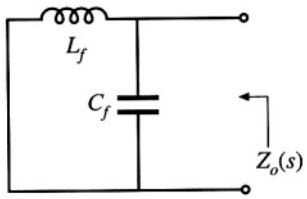

Fig. 10.11 Determination of the filter output impedance $Z_o(s)$.

$$\hat{v}_{test}(s) = -\frac{V_g \hat{d}(s)}{D} \tag{10.22}$$

Insertion of Eqs. (10.21) and (10.22) into Eq. (10.20) leads to the following result:

$$Z_N(s) = \frac{\left(-\dfrac{V_g \hat{d}(s)}{D}\right)}{\left(I\hat{d}(s)\right)} = -\frac{R}{D^2} \tag{10.23}$$

The steady-state relationship $I = DV_g/R$ has been used to simplify the above result. This equation coincides with the expression listed in Table 10.1. The Bode diagram of $\| Z_N(j\omega) \|$ is constructed in Fig. 10.10; this plot coincides with the dc asymptote of $\| Z_D(j\omega) \|$.

Next, let us construct the Bode diagram of the filter output impedance $Z_o(s)$. When the independent source $\hat{v}_g(s)$ is set to zero, the input filter network reduces to the circuit of Fig. 10.11. It can be seen that $Z_o(s)$ is given by the parallel combination of the inductor L_f and the capacitor C_f:

$$Z_o(s) = sL_f \| \frac{1}{sC_f} \tag{10.24}$$

Construction of the Bode diagram of this parallel resonant circuit is discussed in Section 8.3.4. As illustrated in Fig. 10.12, the magnitude $\| Z_o(j\omega) \|$ is dominated by the inductor impedance at low frequency, and by the capacitor impedance at high frequency. The inductor and capacitor asymptotes intersect at the filter resonant frequency:

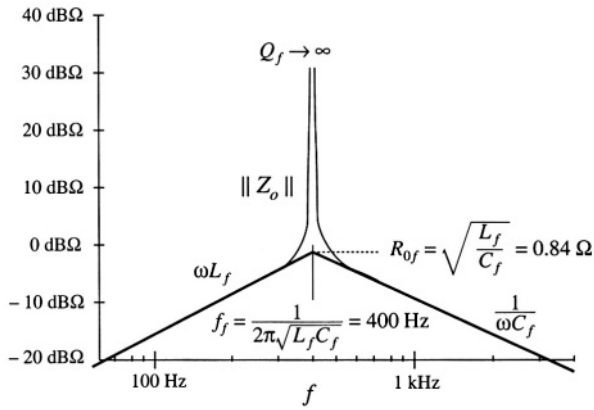

Fig. 10.12 Magnitude plot of the output impedance of the input filter of Fig. 10.11. Since the filter is not damped, the Q-factor is very large.

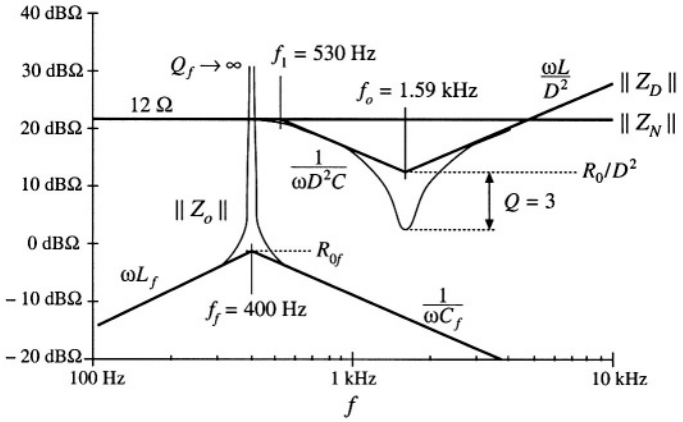

Fig. 10.13 Impedance design criteria $\| Z_N(j\omega) \|$ and $\| Z_D(j\omega) \|$ from Fig. 10.10, with the filter output impedance $\| Z_o(j\omega) \|$ of Fig. 10.12 superimposed. The design criteria of Eq. (10.13) are not satisfied at the input filter resonance.

$$f_f = \frac{1}{2\pi\sqrt{L_f C_f}} \tag{10.25}$$

For the given values, the input filter resonant frequency is $f_f = 400$ Hz. This filter has characteristic impedance

$$R_{0f} = \sqrt{\frac{L_f}{C_f}} \tag{10.26}$$

equal to 0.84 Ω. Since the input filter is undamped, its Q-factor is ideally infinite. In practice, parasitic elements such as inductor loss and capacitor equivalent series resistance limit the value of Q_f. Nonetheless, the impedance $\| Z_o(j\omega) \|$ is very large in the vicinity of the filter resonant frequency f_f.

The Bode plot of the filter output impedance $\| Z_o(j\omega) \|$ is overlaid on the $\| Z_N(j\omega) \|$ and $\| Z_D(j\omega) \|$ plots in Fig. 10.13, for the element values listed in Fig. 10.8(a). We can now determine whether the impedance inequalities (10.13) are satisfied. Note the design-oriented nature of Fig. 10.13: since analytical expressions are given for each impedance asymptote, the designer can easily adjust the component values to satisfy Eq. (10.13). For example, the values of L_f and C_f should be chosen to ensure that the asymptotes of $\| Z_o(j\omega) \|$ lie below the worst-case value of R/D^2, as well as the other asymptotes of $\| Z_D(j\omega) \|$.

It should also be apparent that it is a bad idea to choose the input and output filter resonant frequencies f_0 and f_f to be equal, because it would then be more difficult to satisfy the inequalities of Eq. (10.13). Instead, the resonant frequencies f_0 and f_f should be well separated in value.

Since the input filter is undamped, it is impossible to satisfy the impedance inequalities (10.13) in the vicinity of the input filter resonant frequency f_f. Regardless of the choice of element values, the input filter changes the control-to-output transfer function $G_{vd}(s)$ in the vicinity of frequency f_f. Figures 10.14 and 10.15 illustrate the resulting correction factor [Eq. (10.12)] and the modified control-to-output transfer function [Eq. (10.4)], respectively. At frequencies well below the input filter resonant frequency, impedance inequalities (10.13) are well satisfied. The correction factor tends to the value $1\angle 0°$, and the

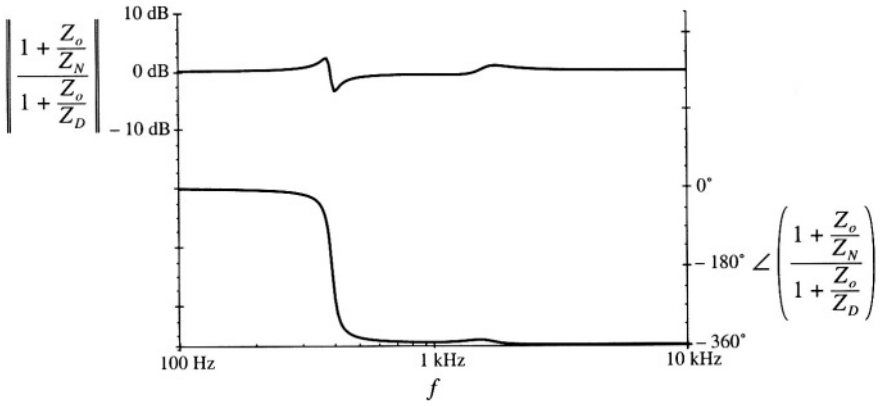

Fig. 10.14 Magnitude of the correction factor, Eq. (10.12), for the buck converter example of Fig. 10.8.

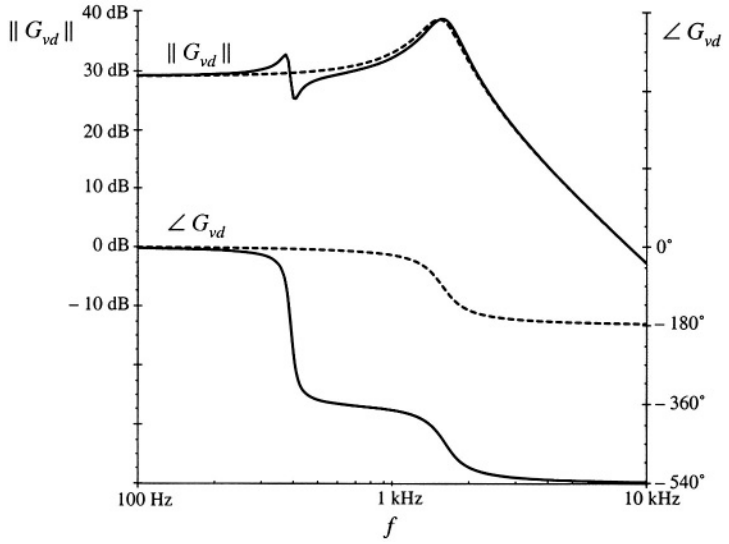

Fig. 10.15 Effect of the undamped input filter on the control-to-output transfer function of the buck converter example. *Dashed lines:* without input filter. *Solid lines:* with undamped input filter.

control-to-output transfer function $G_{vd}(s)$ is essentially unchanged. In the vicinity of the resonant frequency f_f, the correction factor contains a pair of complex poles, and also a pair of right half-plane complex zeroes. These cause a "glitch" in the magnitude plot of the correction factor, and they contribute 360° of lag to the phase of the correction factor. The glitch and its phase lag can be seen in the Bode plot of $G_{vd}(s)$. At high frequency, the correction factor tends to a value of approximately $1\angle -360°$; consequently, the high-frequency magnitude of G_{vd} is unchanged. However, when the – 360° contributed by the correction factor is added to the – 180° contributed at high frequency by the two poles of the original $G_{vd}(s)$, a high-frequency phase asymptote of – 540° is obtained. If the crossover frequency of the converter feedback loop is placed near to or greater than the input filter resonant frequency f_f, then a negative

phase margin is inevitable. This explains why addition of an input filter often leads to instabilities and oscillations in switching regulators.

10.3.2 Damping the Input Filter

Let's damp the resonance of the input filter, so that impedance inequalities (10.13) are satisfied at all frequencies.

One approach to damping the filter is to add resistor R_f in parallel with capacitor C_f as illustrated in Fig. 10.16(a). The output impedance of this network is identical to the parallel resonant impedance analyzed in Section 8.3.4. The maximum value of the output impedance occurs at the resonant frequency f_f, and is equal in value to the resistance R_f. Hence, to satisfy impedance inequalities (10.13), we should choose R_f to be much less than the $\| Z_N(j\omega) \|$ and $\| Z_D(j\omega) \|$ asymptotes. The condition $R_f \ll \| Z_N(j\omega) \|$ can be expressed as:

$$R_f \ll \frac{R}{D^2} \tag{10.27}$$

Unfortunately, this raises a new problem: the power dissipation in R_f. The dc input voltage V_g is applied across resistor R_f, and therefore R_f dissipates power equal to V_g^2/R_f. Equation (10.27) implies that this power loss is greater than the load power! Therefore, the circuit of Fig. 10.16(a) is not a practical solution.

One solution to the power loss problem is to place R_f in parallel with L_f as illustrated in Fig. 10.16(b). The value of R_f in Fig. 10.16(b) is also chosen according to Eq. (10.27). Since the dc voltage across inductor L_f is zero, there is now no dc power loss in resistor R_f. The problem with this circuit is that its transfer function contains a high-frequency zero. Addition of R_f degrades the slope of the high-frequency asymptote, from – 40 dB/decade to – 20 dB/decade. The circuit of Fig. 10.16(b) is effectively a single-pole *R-C* low-pass filter, with no attenuation provided by inductor L_f.

One practical solution is illustrated in Fig. 10.17 [10]. Dc blocking capacitor C_b is added in series with resistor R_f. Since no dc current can flow through resistor R_f, its dc power loss is eliminated. The value of C_b is chosen to be very large such that, at the filter resonant frequency f_f, the impedance of the R_f-C_b branch is dominated by resistor R_f. When C_b is sufficiently large, then the output impedance of this network reduces to the output impedances of the filters of Fig. 10.16. The impedance asymptotes for the case of large C_b are illustrated in Fig. 10.17(b).

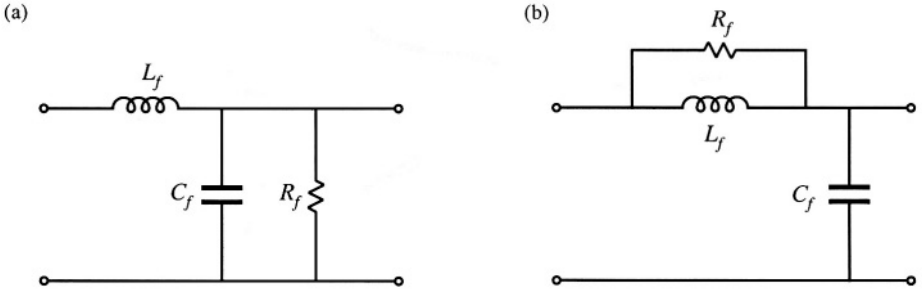

Fig. 10.16 Two attempts to damp the input filter: (a) addition of damping resistance R_f across C_f, (b) addition of damping resistance R_f in parallel with L_f.

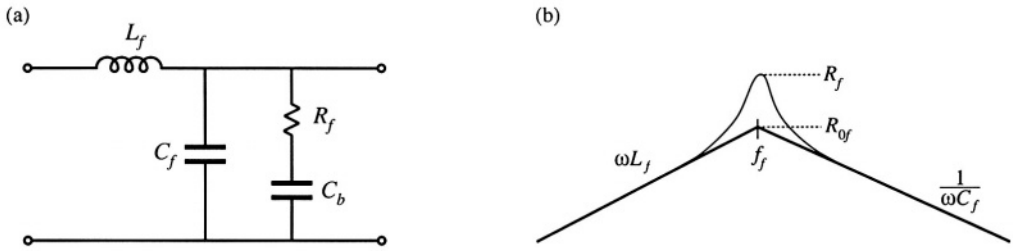

Fig. 10.17 A practical method to damping the input filter, including damping resistance R_f and dc blocking capacitor C_b: (a) circuit, (b) output impedance asymptotes.

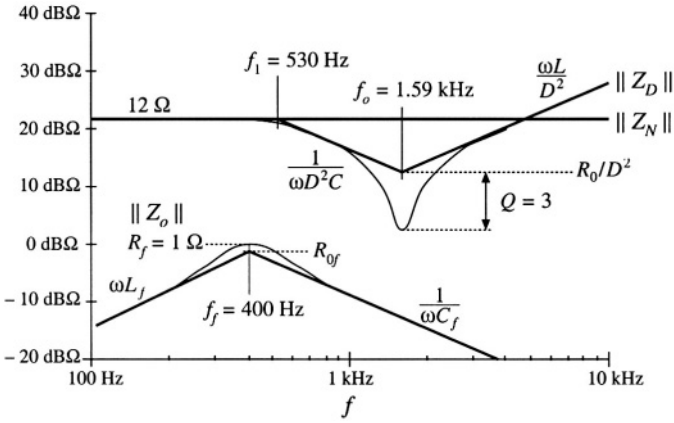

Fig. 10.18 Impedance design criteria $\| Z_N(j\omega) \|$ and $\| Z_D(j\omega) \|$ from Fig. 10.10, with the filter output impedance $\| Z_o(j\omega) \|$ of Fig. 10.17(b) superimposed. The design criteria of Eq. (10.13) are well satisfied.

The low-frequency asymptotes of $\| Z_N(j\omega) \|$ and $\| Z_D(j\omega) \|$ in Fig. 10.10 are equal to $R/D^2 = 12\ \Omega$. The choice $R_f = 1\ \Omega$ therefore satisfies impedance inequalities (10.13) very well. The choice $C_b = 4700\ \mu\text{F}$ leads to $1/2\pi f_f C_b = 0.084\ \Omega$, which is much smaller than R_f. The resulting magnitude $\| Z_o(j\omega) \|$ is compared with $\| Z_N(j\omega) \|$ and $\| Z_D(j\omega) \|$ in Fig. 10.18. It can be seen that the chosen values of R_f and C_b lead to adequate damping, and impedance inequalities (10.13) are now well satisfied.

Figure 10.19 illustrates how addition of the damped input filter modifies the magnitude and phase of the control-to-output transfer function. There is now very little change in $G_{vd}(s)$, and we would expect that the performance of the converter feedback loop is unaffected by the input filter.

10.4 DESIGN OF A DAMPED INPUT FILTER

As illustrated by the example of the previous section, design of an input filter requires not only that the filter impedance asymptotes satisfy impedance inequalities, but also that the filter be adequately damped. Damping of the input filter is also necessary to prevent transients and disturbances in $v_g(t)$ from exciting filter resonances. Other design constraints include attaining the desired filter attenuation, and minimizing

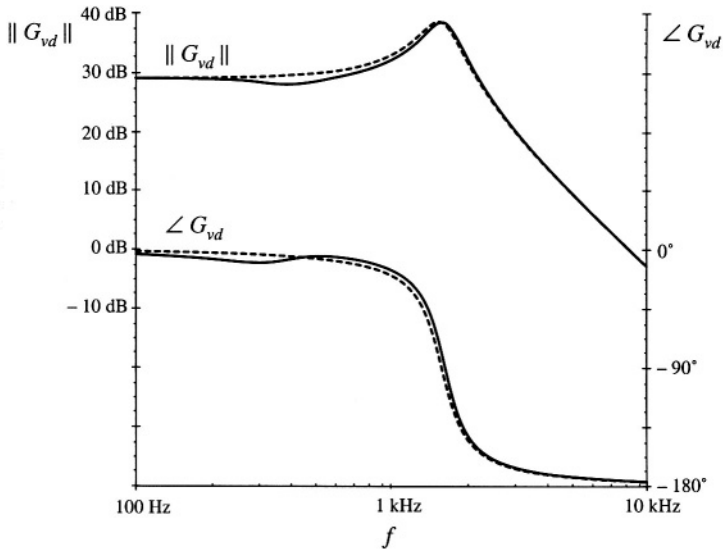

Fig. 10.19 Effect of the damped input filter on the control-to-output transfer function of the buck converter example. *Dashed lines:* without input filter. *Solid lines:* with damped input filter.

the size of the reactive elements. Although a large number of classical filter design techniques are well known, these techniques do not address the problems of limiting the maximum output impedance and damping filter resonances.

The value of the blocking capacitor C_b used to damp the input filter in Section 10.3.2 is ten times larger than the value of C_f, and hence its size and cost are of practical concern. Optimization of an input filter design therefore includes minimization of the size of the elements used in the damping networks.

Several practical approaches to damping the single-section *L-C* low-pass filter are illustrated in Fig. 10.20 [10,11,17]. Figure 10.20(a) contains the R_f-C_b damping branch considered in the previous section. In Fig. 10.20(b), the damping resistor R_f is placed in parallel with the filter inductor L_f, and a high-frequency blocking inductor L_b is placed in series with R_f. Inductor L_b causes the filter transfer function to roll off with a high-frequency slope of – 40 dB/decade. In Fig. 10.20(c), the damping resistor R_f is placed in series with the filter inductor L_f, and the dc current is bypassed by inductor L_b. In each case, it is desired to obtain a given amount of damping [i.e., to cause the peak value of the filter output impedance to be no greater than a given value that satisfies the impedance inequalities (10.13)], while minimizing the value of C_b or L_b. This problem can be formulated in an alternate but equivalent form: for a given choice of C_b or L_b findthe value of R_f that minimizes the peak output impedance [10]. The solutions to this optimization problem, for the three filter networks of Fig. 21, are summarized in this section. In each case, the quantities R_{0f} and f_f are defined by Eqs. (10.25) and (10.26).

Consider the filter of Fig. 10.20(b), with fixed values of L_f, C_f, and L_b. Figure 10.21 contains Bode plots of the filter output impedance $\| Z_o(j\omega) \|$ for several values of damping resistance R_f. For the limiting case $R_f = \infty$, the circuit reduces to the original undamped filter with infinite Q_f. In the limiting case $R_f = 0$, the filter is also undamped, but the resonant frequency is increased because L_b becomes connected in parallel with L_f. Between these two extremes, there must exist an optimum value of R_f that causes the peak filter output impedance to be minimized. It can be shown [10,17] that all magnitude plots must pass through a common point, and therefore the optimum attains its peak at this point. This fact has been used to derive the design equations of optimally-damped *L-C* filter sections.

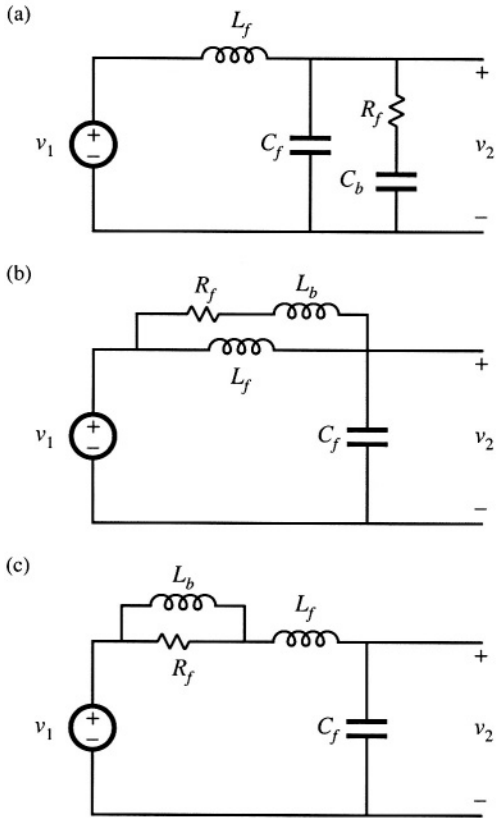

Fig. 10.20 Several practical approaches to damping the single-section input filter: (a) R_f-C_b parallel damping, (b) R_f-L_b parallel damping, (c) R_f-L_b series damping.

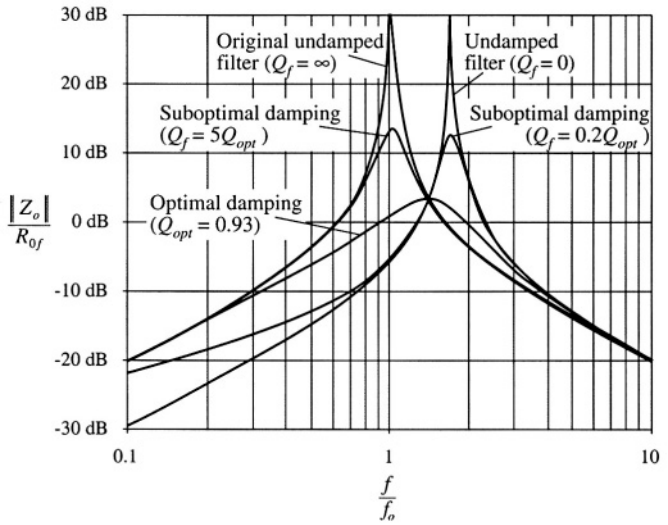

Fig. 10.21 Comparison of output impedance curves for optimal parallel R_f-L_b damping with undamped and several suboptimal designs. For this example, $n = L_b/L = 0.516$

10.4.1 R_f-C_b Parallel Damping

Optimization of the filter network of Fig. 10.20(a) and Section 10.3.2 was described in [10]. The high-frequency attenuation of this filter is not affected by the choice of C_b, and the high-frequency asymptote is identical to that of the original undamped filter. The sole tradeoff in design of the damping elements for this filter is in the size of the blocking capacitor C_b vs. the damping achieved.

For this filter, let us define the quantity n as the ratio of the blocking capacitance C_b to the filter capacitance C_f:

$$n = \frac{C_b}{C_f} \tag{10.28}$$

For the optimum design, the peak filter output impedance occurs at the frequency

$$f_m = f_f \sqrt{\frac{2}{2+n}} \tag{10.29}$$

The value of the peak output impedance for the optimum design is

$$\| Z_o \|_{mm} = R_{0f} \frac{\sqrt{2(2+n)}}{n} \tag{10.30}$$

The value of damping resistance that leads to optimum damping is described by

$$Q_{opt} = \frac{R_f}{R_{0f}} = \sqrt{\frac{(2+n)(4+3n)}{2n^2(4+n)}} \tag{10.31}$$

The above equations allow choice of the damping values R_f and C_b.

For example, let's redesign the damping network of Section 10.3.2, to achieve the same peak output impedance $\| Z_o(j\omega) \|_{mm} = 1\ \Omega$, while minimizing the value of the blocking capacitance C_b. From Section 10.3.2, the other parameter values are $R_{0f} = 0.84\ \Omega$, $C_f = 470\ \mu F$, and $L_f = 330\ \mu H$. First, we solve Eq. (10.30) to find the required value of n:

$$n = \frac{R_{0f}^2}{\| Z_o \|_{mm}^2} \left(1 + \sqrt{1 + 4 \frac{\| Z_o \|_{mm}^2}{R_{0f}^2}} \right) \tag{10.32}$$

Evaluation of this expression with the given numerical values leads to $n = 2.5$. The blocking capacitor is therefore required to have a value of $nC_f = 1200\ \mu F$. This is one-quarter of the value employed in Section 10.3.2. The value of R_f is then found by evaluation of Eq. (10.31), leading to

$$R_f = R_{0f} \sqrt{\frac{(2+n)(4+3n)}{2n^2(4+n)}} = 0.67\ \Omega \tag{10.33}$$

The output impedance of this filter design is compared with the output impedances of the original undamped filter of Section 10.3.1, and of the suboptimal design of Section 10.3.2, in Fig. 10.22. It can be

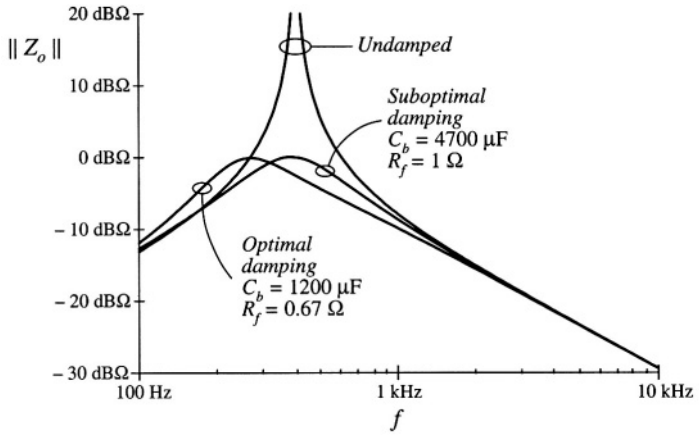

Fig. 10.22 Comparison of the output impedances of the design with optimal parallel R_f-C_b damping, the suboptimal design of Section 10.3.2, and the original undamped filter.

seen that the optimally damped filter does indeed achieve the desired peak output impedance of 1 Ω, at the slightly lower peak frequency given by Eq. (10.29)

The R_f-C_b parallel damping approach finds significant application in dc–dc converters. Since a series resistor is placed in series with C_b, C_b can be realized using capacitor types having substantial equivalent series resistance, such as electrolytic and tantalum types. However, in some applications, the R_f-L_b approaches of the next subsections can lead to smaller designs. Also, the large blocking capacitor value may be undesirable in applications having an ac input.

10.4.2 R_f-L_b Parallel Damping

Figure 10.20(b) illustrates the placement of damping resistor R_f in parallel with inductor L_f. Inductor L_b causes the filter to exhibit a two-pole attenuation characteristic at high frequency. To allow R_f to damp the filter, inductor L_b should have an impedance magnitude that is sufficiently smaller than R_f at the filter resonant frequency f_f. Optimization of this damping network is described in [17].

With this approach, inductor L_b can be physically much smaller than L_f. Since R_f is typically much greater than the dc resistance of L_f, essentially none of the dc current flows through L_b. Furthermore, R_f could be realized as the equivalent series resistance of L_b at the filter resonant frequency f_f. Hence, this is a very simple, low-cost approach to damping the input filter.

The disadvantage of this approach is the fact that the high-frequency attenuation of the filter is degraded: the high-frequency asymptote of the filter transfer function is increased from $1/\omega^2 L_f C_f$ to $1/\omega^2 (L_f \| L_b) C_f$. Furthermore, since the need for damping limits the maximum value of L_b, significant loss of high-frequency attenuation is unavoidable. To compensate, the value of L_f must be increased. Therefore, a tradeoff occurs between damping and degradation of high-frequency attenuation, as illustrated in Fig. 10.23. For example, limiting the degradation of high-frequency attenuation to 6 dB leads to an optimum peak filter output impedance $\| Z_o \|_{mm}$ of $\sqrt{6}$ times the original characteristic impedance R_{0f}. Additional damping leads to further degradation of the high-frequency attenuation.

The optimally damped design (i.e., the choice of R_f that minimizes the peak output impedance

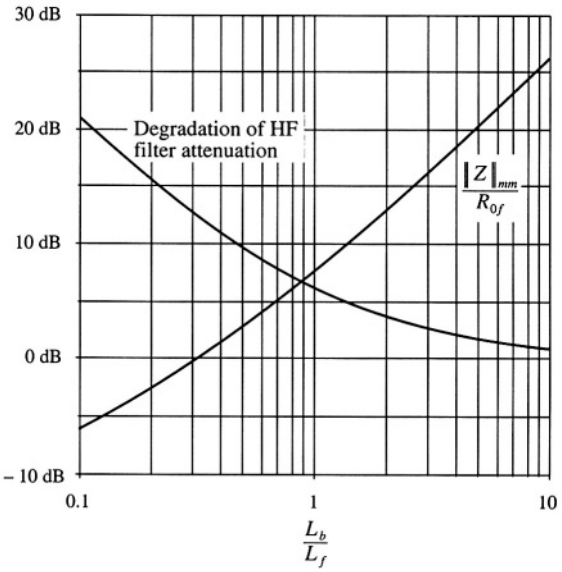

Fig. 10.23 Performance attained via optimal design procedure, parallel R_f-L_b circuit of 10.20(b). Optimum peak filter output impedance $\| Z_o \|_{mm}$ and increase of filter high-frequency gain, vs. $n = L_b/L$.

$\| Z_o \|$ for a given choice of L_b) is described by the following equations:

$$Q_{opt} = \frac{R_f}{R_{0f}} = \sqrt{\frac{n(3+4n)(1+2n)}{2(1+4n)}} \tag{10.34}$$

where

$$n = \frac{L_b}{L_f} \tag{10.35}$$

The peak filter output impedance occurs at frequency

$$f_m = f_f \sqrt{\frac{1+2n}{2n}} \tag{10.36}$$

and has the value

$$\|Z_o\|_{mm} = R_{0f} \sqrt{2n(1+2n)} \tag{10.37}$$

The attenuation of the filter high-frequency asymptote is degraded by the factor

$$\frac{L_f}{L_f \| L_b} = 1 + \frac{1}{n} \tag{10.38}$$

So, given an undamped L_f-C_f filter having corner frequency f_f, and characteristic impedance R_{0f}, and given a requirement for the maximum allowable output impedance $\| Z_o \|_{mm}$, one can solve Eq. (10.37) for the required value of n. One can then determine the required numerical values of L_b and R_f.

10.4.3 R_f-L_b Series Damping

Figure 10.20(c) illustrates the placement of damping resistor R_f in series with inductor L_f. Inductor L_b provides a dc bypass to avoid significant power dissipation in R_f. To allow R_f to damp the filter, inductor L_b should have an impedance magnitude that is sufficiently greater than R_f at the filter resonant frequency.

Although this circuit is theoretically equivalent to the parallel damping R_f-L_b case of Section 10.4.2, several differences are observed in practical designs. Both inductors must carry the full dc current, and hence both have significant size. The filter high-frequency attenuation is not affected by the choice of L_b, and the high-frequency asymptote is identical to that of the original undamped filter. The tradeoff in design of this filter does not involve high-frequency attenuation; rather, the issue is damping vs. bypass inductor size.

Design equations similar to those of the previous sections can be derived for this case. The optimum peak filter output impedance occurs at frequency

$$f_m = f_f \sqrt{\frac{2+n}{2(1+n)}} \tag{10.39}$$

and has the value

$$\|Z_o\|_{max} = R_{0f} \frac{\sqrt{2(1+n)(2+n)}}{n} \tag{10.40}$$

The value of damping resistance that leads to optimum damping is described by

$$Q_{opt} = \frac{R_{0f}}{R_f} = \left(\frac{1+n}{n}\right) \sqrt{\frac{2(1+n)(4+n)}{(2+n)(4+3n)}} \tag{10.41}$$

For this case, the peak output impedance cannot be reduced below $\sqrt{2}\,R_{0f}$ via damping. Nonetheless, it is possible to further reduce the filter output impedance by redesign of L_f and C_f, to reduce the value of R_{0f}.

10.4.4 Cascading Filter Sections

A cascade connection of multiple *L-C* filter sections can achieve a given high-frequency attenuation with less volume and weight than a single-section *L-C* filter. The increased cutoff frequency of the multiple-section filter allows use of smaller inductance and capacitance values. Damping of each *L-C* section is usually required, which implies that damping of each section should be optimized. Unfortunately, the results of the previous sections are restricted to single-section filters. Interactions between cascaded *L-C* sections can lead to additional resonances and increased filter output impedance.

It is nonetheless possible to design cascaded filter sections such that interaction between *L-C* sections is negligible. In the approach described below, the filter output impedance is approximately equal to the output impedance of the last section, and resonances caused by interactions between stages are avoided. Although the resulting filter may not be "optimal" in any sense, insight can be gained that allows intelligent design of multiple-section filters with economical damping of each section.

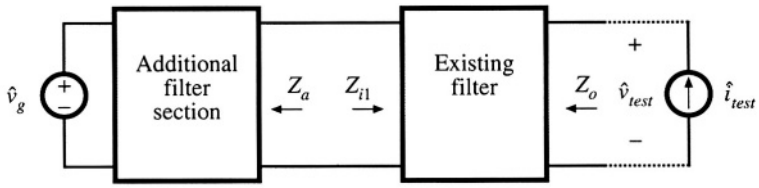

Fig. 10.24 Addition of a filter section at the input of an existing filter.

Consider the addition of a filter section to the input of an existing filter, as in Fig. 10.24. Let us assume that the existing filter has been correctly designed to meet the output impedance design criteria of Eq. (10.13): under the conditions $Z_a(s) = 0$ and $\hat{v}_g(s) = 0$, $\| Z_o \|$ is sufficiently small. It is desired to add a damped filter section that does not significantly increase $\| Z_o \|$.

Middlebrook's extra element theorem of Appendix C can again be invoked, to express how addition of the filter section modifies $Z_o(s)$:

$$\text{modified } Z_o(s) = \left[Z_o(s) \right]_{Z_a(s)=0} \frac{\left(1 + \dfrac{Z_a(s)}{Z_{N1}(s)} \right)}{\left(1 + \dfrac{Z_a(s)}{Z_{D1}(s)} \right)} \tag{10.42}$$

where

$$Z_{N1}(s) = Z_{i1}(s) \Big|_{\hat{v}_{test}(s) \to 0 \text{ null}} \tag{10.43}$$

is the impedance at the input port of the existing filter, with its output port short-circuited. Note that, in this particular case, nulling $\hat{v}_{test}(s)$ is the same as shorting the filter output port because the short-circuit current flows through the $\hat{i}_{test}$ source. The quantity

$$Z_{D1}(s) = Z_{i1}(s) \Big|_{\hat{i}_{test}(s)=0} \tag{10.44}$$

is the impedance at the input port of the existing filter, with its output port open-circuited. Hence, the additional filter section does not significantly alter Z_o provided that

$$\begin{aligned} |Z_a| &\ll |Z_{N1}| \quad \text{and} \\ |Z_a| &\ll |Z_{D1}| \end{aligned} \tag{10.45}$$

Bode plots of the quantities Z_{N1} and Z_{D1} can be constructed either analytically or by computer simulation, to obtain limits of Z_a. When $\| Z_a \|$ satisfies Eq. (10.45), then the "correction factor" $(1 + Z_a/Z_{N1})/(1 + Z_a/Z_{D1})$ is approximately equal to 1, and the modified Z_o is approximately equal to the original Z_o.

To satisfy the design criteria (10.45), it is advantageous to select the resonant frequencies of Z_a to differ from the resonant frequencies of Z_{D1}. In other words, we should stagger-tune the filter sections. This minimizes the interactions between filter sections, and can allow use of smaller reactive element values.

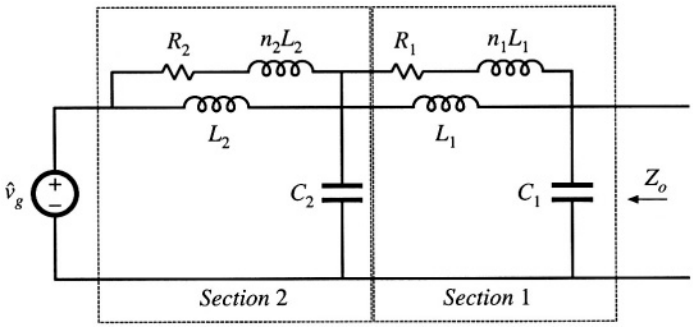

Fig. 10.25 Two-section input filter example, employing R_f-L_b parallel damping in each section.

10.4.5 Example: Two Stage Input Filter

As an example, let us consider the design of a two-stage filter using R_f-L_b parallel damping in each section as illustrated in Fig. 10.25 [17]. It is desired to achieve the same attenuation as the single-section filters designed in Sections 10.3.2 and 10.4.1, and to filter the input current of the same buck converter example of Fig. 10.8. These filters exhibit an attenuation of 80 dB at 250 kHz, and satisfy the design inequalities of Eq. (10.13) with the $\| Z_N \|$ and $\| Z_D \|$ impedances of Fig. 10.10. Hence, let's design the filter of Fig. 10.25 to attain 80 dB of attenuation at 250 kHz.

As described in the previous section and below, it is advantageous to stagger-tune the filter sections so that interaction between filter sections is reduced. We will find that the cutoff frequency of filter section 1 should be chosen to be smaller than the cutoff frequency of section 2. In consequence, the attenuation of section 1 will be greater than that of section 2. Let us (somewhat arbitrarily) design to obtain 45 dB of attenuation from section 1, and 35 dB of attenuation from section 2 (so that the total is the specified 80 dB). Let us also select $n_1 = n_2 = n = L_b/L_f = 0.5$ for each section; as illustrated in Fig. 10.23, this choice leads to a good compromise between damping of the filter resonance and degradation of high frequency filter attenuation. Equation (10.38) and Fig. 10.23 predict that the R_f-L_b damping network will degrade the high frequency attenuation by a factor of $(1 + 1/n) = 3$, or 9.5 dB. Hence, the section 1 undamped resonant frequency f_{f1} should be chosen to yield 45 dB + 9.5 dB = 54.5 dB $\Rightarrow$ 533 of attenuation at 250 kHz. Since section 1 exhibits a two-pole (– 40 dB/decade) roll-off at high frequencies, f_{f1} should be chosen as follows:

$$f_{f1} = \frac{(250\ \text{kHz})}{\sqrt{533}} = 10.8\ \text{kHz} \tag{10.46}$$

Note that this frequency is well above the 1.6 kHz resonant frequency f_0 of the buck converter output filter. Consequently, the output impedance $\| Z_o \|$ can be as large as 3 Ω, and still be well below the $\| Z_N(j\omega) \|$ and $\| Z_D(j\omega) \|$ plots of Fig. 10.10.

Solution of Eq. (10.37) for the required section 1 characteristic impedance that leads to a peak output impedance of 3 Ω with $n = 0.5$ leads to

$$R_{0f1} = \frac{|Z_o|_{mm}}{\sqrt{2n(1+2n)}} = \frac{3\ \Omega}{\sqrt{2(0.5)(1+2(0.5))}} = 2.12\ \Omega \tag{10.47}$$

The filter inductance and capacitance values are therefore

$$L_1 = \frac{R_{0f1}}{2\pi f_{f1}} = 31.2\ \mu H$$
$$C_1 = \frac{1}{2\pi f_{f1} R_{0f1}} = 6.9\ \mu F \tag{10.48}$$

The section 1 damping network inductance is

$$n_1 L_1 = 15.6\ \mu H \tag{10.49}$$

The section 1 damping resistance is found from Eq. (10.34):

$$R_1 = Q_{opt} R_{0f1} = R_{0f1} \sqrt{\frac{n(3+4n)(1+2n)}{2(1+4n)}} = 1.9\ \Omega \tag{10.50}$$

The peak output impedance will occur at the frequency given by Eq. (10.36), 15.3 kHz. The quantities $\| Z_{N1}(j\omega) \|$ and $\| Z_{D1}(j\omega) \|$ for filter section 1 can now be constructed analytically or plotted by computer simulation. $\| Z_{N1}(j\omega) \|$ is the section 1 input impedance Z_{i1} with the output of section 1 shorted, and is given by the parallel combination of the sL_1 and the $(R_1 + sn_1L_1)$ branches. $\| Z_{D1}(j\omega) \|$ is the section 1 input impedance Z_{i1} with the output of section 1 open-circuited, and is given by the series combination of $Z_{N1}(s)$ with the capacitor impedance $1/sC_1$. Figure 10.26 contains plots of $\| Z_{N1}(j\omega) \|$ and $\| Z_{D1}(j\omega) \|$ for filter section 1, generated using Spice.

One way to approach design of filter section 2 is as follows. To avoid significantly modifying the overall filter output impedance Z_o, the section 2 output impedance $\| Z_a(j\omega) \|$ must be sufficiently less than $\| Z_{N1}(j\omega) \|$ and $\| Z_{D1}(j\omega) \|$. It can be seen from Fig. 10.26 that, with respect to $\| Z_{D1}(j\omega) \|$, this is most difficult to accomplish when the peak frequencies of sections 1 and 2 coincide. It is most difficult to satisfy the $\| Z_{N1}(j\omega) \|$ design criterion when the peak frequency of sections 2 is lower than the peak frequency of section 1. Therefore, the best choice is to stagger-tune the filter sections, with the resonant frequency of section 1 being lower than the peak frequency of section 2. This implies that section 1 will produce more high-frequency attenuation than section 2. For this reason, we have chosen to achieve 45 dB of attenuation with section 1, and 35 dB of attenuation from section 2.

The section 2 undamped resonant frequency f_{f2} should be chosen in the same manner used in Eq. (10.46) for section 1. We have chosen to select $n_2 = n = L_b/L_f = 0.5$ for section 2; this again means that the R_f-L_b damping network will degrade the high frequency attenuation by a factor of $(1 + 1/n) = 3$, or 9.5 dB. Hence, the section 2 undamped resonant frequency f_{f2} should be chosen to yield 35 dB + 9.5 dB = 44.5 dB $\Rightarrow$ 169 of attenuation at 250 kHz. Since section 2 exhibits a two-pole (– 40 dB/decade) roll-off at high frequencies, f_{f2} should be chosen as follows:

$$f_{f2} = \frac{(250\ kHz)}{\sqrt{169}} = 19.25\ kHz \tag{10.51}$$

The output impedance of section 2 will peak at the frequency 27.2 kHz, as given by Eq. (10.36). Hence, the peak frequencies of sections 1 and 2 differ by almost a factor of 2.

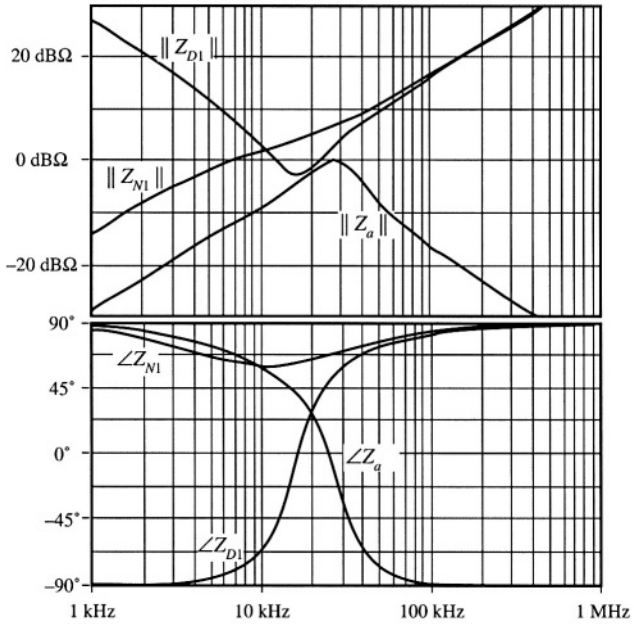

Fig. 10.26 Bode plot of Z_{N1} and Z_{D1} for filter section 1. Also shown is the Bode plot for the output impedance Z_a of filter section 2.

Figure 10.26 shows that, at 27.2 kHz, $\| Z_{D1}(j\omega) \|$ has a magnitude of roughly 3 dBΩ, and that $\| Z_{N1}(j\omega) \|$ is approximately 7 dBΩ. Hence, let us design section 2 to have a peak output impedance of 0 dBΩ ⇒ 1 Ω. Solution of Eq. (10.37) for the required section 2 characteristic impedance leads to

$$R_{0f2} = \frac{\| Z_a \|_{mm}}{\sqrt{2n\left(1+2n\right)}} = \frac{1\ \Omega}{\sqrt{2(0.5)\left(1+2(0.5)\right)}} = 0.71\ \Omega \tag{10.52}$$

The section 2 element values are therefore

$$\begin{aligned} L_2 &= \frac{R_{0f2}}{2\pi f_{f2}} = 5.8\ \mu\text{H} \\ C_2 &= \frac{1}{2\pi f_{f2} R_{0f2}} = 11.7\ \mu\text{F} \\ n_2 L_2 &= 2.9\ \mu\text{H} \\ R_2 &= Q_{opn} R_{0f2} = R_{0f2}\sqrt{\frac{n\left(3+4n\right)\left(1+2n\right)}{2\left(1+4n\right)}} = 0.65\ \Omega \end{aligned} \tag{10.53}$$

A Bode plot of the resulting Z_a is overlaid on Fig. 10.26. It can be seen that $\| Z_a(j\omega) \|$ is less than, but very close to, $\| Z_{D1}(j\omega) \|$ between the peak frequencies of 15 kHz and 27 kHz. The impedance inequalities (10.45) are satisfied somewhat better below 15 kHz, and are satisfied very well at high frequency.

The resulting filter output impedance $\| Z_o(j\omega) \|$ is plotted in Fig. 10.27, for section 1 alone and for the complete cascaded two-section filter. It can be seen that the peak output impedance is approxi-

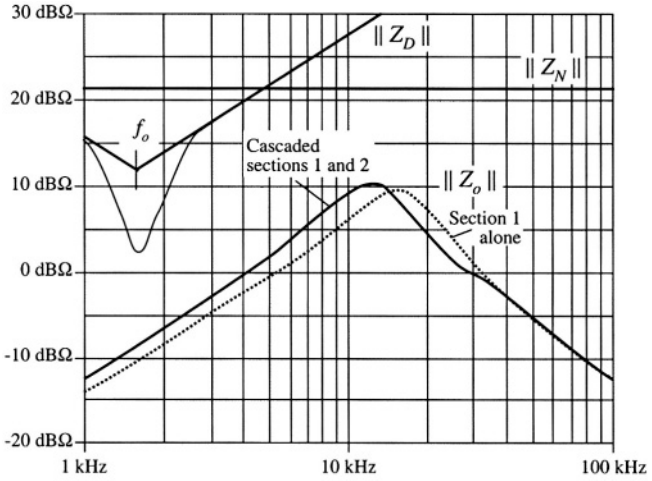

Fig. 10.27 Comparison of the impedance design criteria $\| Z_N(j\omega) \|$ and $\| Z_D(j\omega) \|$, Eq. (10.13), with the filter output impedance $\| Z_o(j\omega) \|$. *Solid line:* $\| Z_o(j\omega) \|$ of cascaded design. *Dashed line:* $\| Z_o(j\omega) \|$ of section 1 alone.

mately 10 dBΩ, or roughly 3 Ω. The impedance design criteria (10.13) are also shown, and it can be seen that the filter meets these design criteria. Note the absence of resonances in $\| Z_o(j\omega) \|$.

The effect of stage 2 on $\| Z_o(j\omega) \|$ is very small above 40 kHz [where inequalities (10.45) are very well satisfied], and has moderate-to-small effect at lower frequencies. It is interesting that, above approximately 12 kHz, the addition of stage 2 actually *decreases* $\| Z_o(j\omega) \|$. The reason for this can be seen from Fig. C.8 of Appendix C: when the phase difference between $\angle Z_a(j\omega)$ and $\angle Z_{D1}(j\omega)$ is not too large ($\leq 90°$), then the $1/(1 + Z_a/Z_{D1})$ term decreases the magnitude of the resulting $\| Z_o(j\omega) \|$. As can be seen from the phase plot of Fig. 10.26, this is indeed what happens. So allowing $\| Z_a(j\omega) \|$ to be similar in magnitude to $\| Z_{D1}(j\omega) \|$ above 12 kHz was an acceptable design choice.

The resulting filter transfer function is illustrated in Fig. 10.28. It can be seen that it does indeed attain the goal of 80 dB attenuation at 250 kHz.

Figure 10.29 compares the single stage design of Section 10.4.1 to the two-stage design of this section. Both designs attain 80 dB attenuation at 250 kHz, and both designs meet the impedance design criteria of Eq. (10.13). However, the single-stage approach requires much larger filter elements.

10.5 SUMMARY OF KEY POINTS

1. Switching converters usually require input filters, to reduce conducted electromagnetic interference and possibly also to meet requirements concerning conducted susceptibility.
2. Addition of an input filter to a converter alters the control-to-output and other transfer functions of the converter. Design of the converter control system must account for the effects of the input filter.
3. If the input filter is not damped, then it typically introduces complex poles and RHP zeroes into the converter control-to-output transfer function, at the resonant frequencies of the input filter. If these resonant frequencies are lower than the crossover frequency of the controller loop gain, then the phase margin will become negative and the regulator will be unstable.

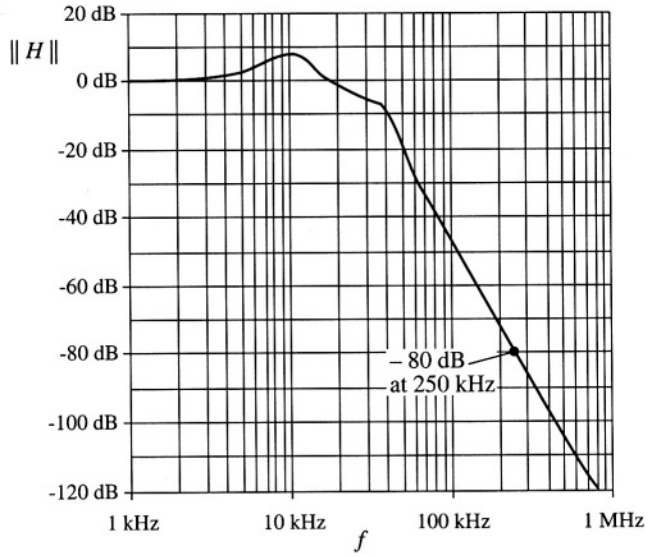

Fig. 10.28 Input filter transfer function, cascaded two-section design.

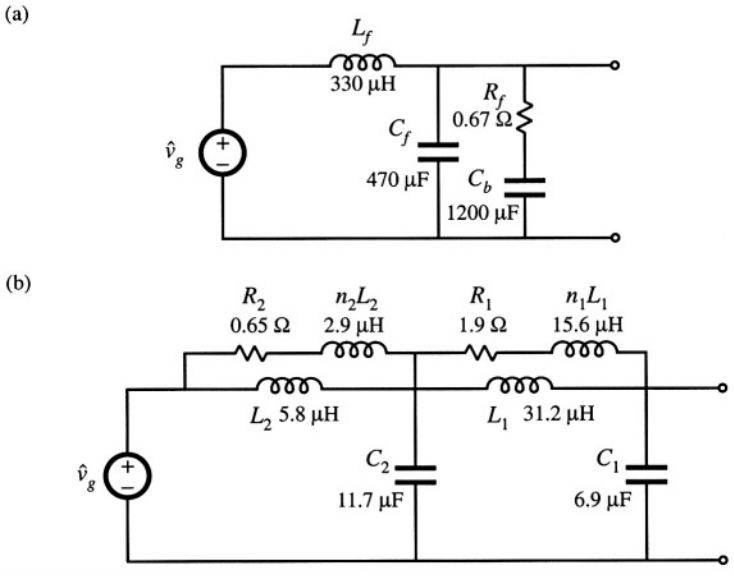

Fig. 10.29 Comparison of single-section (a) and two section (b) input filter designs. Both designs meet the design criteria (10.13), and both exhibit 80 dB of attenuation at 250 kHz.

4. The input filter can be designed so that it does not significantly change the converter control-to-output and other transfer functions. Impedance inequalities (10.13) give simple design criteria that guarantee this. To meet these design criteria, the resonances of the input filter must be sufficiently damped.
5. Optimization of the damping networks of single-section filters can yield significant savings in filter element size. Equations for optimizing three different filter sections are listed.
6. Substantial savings in filter element size can be realized via cascading filter sections. The design of noninteracting cascaded filter sections can be achieved by an approach similar to the original input filter design method. Impedance inequalities (10.45) give design criteria that guarantee that interactions are not substantial.

REFERENCES

[1] M. NAVE, *Power Line Filter Design for Switched Mode Power Supplies,* New York: Van Nostrand Reinhold, 1991.

[2] *Design Guide for Electromagnetic Interference (EMI) Reduction in Power Supplies,* MIL-HDBK-241B, U.S. Department of Defense, April 1 1981.

[3] C. MARSHAM, *The Guide to the EMC Directive 89/336/EEC,* New York: IEEE Press, 1992.

[4] P. DEGAUQUE and J. HAMELIN, *Electromagnetic Compatibility,* Oxford: Oxford University Press, 1993.

[5] R. REDL, "Power Electronics and Electromagnetic Compatibility," *IEEE Power Electronics Specialists Conference,* 1996 Record, pp. 15-21.

[6] P. R. WILLCOCK, J. A. FERREIRA, J. D. VAN WYK, "An Experimental Approach to Investigate the Generation and Propagation of Conducted EMI in Converters," *IEEE Power Electronics Specialists Conference,* 1998 Record, pp. 1140-1146.

[7] L. ROSSETTO, S. BUSO and G. SPIAZZI, "Conducted EMI Issues in a 600W Single-Phase Boost PFC Design," *IEEE Transactions on Industry Applications,* Vol. 36, No. 2, pp. 578-585, March/April 2000.

[8] F. DOS REIS, J. SEBASTIAN and J. UCEDA, "Determination of EMI Emissions in Power Factor Preregulators by Design," *IEEE Power Electronics Specialists Conference,* 1994 Record, pp. 1117-1126.

[9] R. D. MIDDLEBROOK, "Input Filter Considerations in Design and Application of Switching Regulators," *IEEE Industry Applications Society Annual Meeting,* 1976 Record, pp. 366-382.

[10] R. D. MIDDLEBROOK, "Design Techniques for Preventing Input Filter Oscillations in Switched-Mode Regulators," *Proceedings of Powercon 5,* pp. A3.1 – A3.16, May 1978.

[11] T. PHELPS and W. TATE, "Optimizing Passive Input Filter Design," *Proceedings of Powercon 6,* pp. G1.1-G1.10, May 1979.

[12] Y. JANG and R. ERICKSON, "Physical Origins of Input Filter Oscillations in Current Programmed Converters," *IEEE Transactions on Power Electronics,* Vol 7, No. 4, pp. 725-733, October 1992.

[13] S. ERICH and W. POLIVKA, "Input Filter Design for Current-Programmed Regulators," *IEEE Applied Power Electronics Conference,* 1990 Proceedings, pp. 781-791, March 1990.

[14] N. SOKAL, "System Oscillations Caused by Negative Input Resistance at the Power Input Port of a Switching Mode Regulator, Amplifier, Dc/Dc Converter, or Dc/Ac Inverter," *IEEE Power Electronics Specialists Conference,* 1973 Record, pp. 138-140.

[15] A. KISLOVSKI, R. REDL, and N. SOKAL, *Dynamic Analysis of Switching-Mode Dc/Dc Converters,* New York: Van Nostrand Reinhold, Chapter 10, 1991.

[16] S. KELKAR and F. LEE, "A Novel Input Filter Compensation Scheme for Switching Regulators," *IEEE Power Electronics Specialists Conference,* 1982 Record, pp. 260-271.

[17] R. ERICKSON, "Optimal Single-Resistor Damping of Input Filters," *IEEE Applied Power Electronics Conference,* 1999 Proceedings, pp. 1073-1097, March 1999.

[18] M. FLOREZ-LIZARRAGA and A. F. WITULSKI, "InputFilter Design for Multiple-Module DC Power Systems," *IEEE Transactions on Power Electronics,* Vol 11, No. 3, pp. 472-479, May 1996.

[19] V. VLATKOVIĆ, D. BOROJEVIĆ and F. LEE, "Input Filter Design for Power Factor Correction Circuits," *IEEE Transactions on Power Electronics,* Vol 11, No.1, pp. 199-205, January 1996.

[20] F. YUAN, D. Y. CHEN, Y. WU and Y. CHEN, "A Procedure for Designing EMI Filters for Ac Line Applications," *IEEE Transactions on Power Electronics,* Vol 11, No. 1, pp. 170-181, January 1996.

[21] G. SPIAZZI and J. POMILIO, "Interaction Between EMI Filter and Power Factor Preregulators with Average Current Control: Analysis and Design Considerations," *IEEE Transactions on Industrial Electronics,* Vol. 46, No. 3, pp. 577-584, June 1999.

PROBLEMS

10.1 It is required to design an input filter for the flyback converter of Fig. 10.30. The maximum allowed amplitude of switching harmonics of $i_{in}(t)$ is 10 μA rms. Calculate the required attenuation of the filter at the switching frequency.

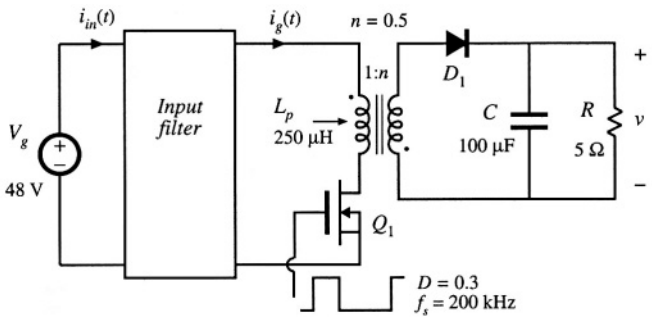

Fig. 10.30 Flyback converter, Problems 10.1, 10.4, 10.6, 10.8, and 10.10.

10.2 In the boost converter of Fig. 10.31, the input filter is designed so that the maximum amplitude of switching harmonics of $i_{in}(t)$ is not greater than 10 μA rms. Find the required attenuation of the filter at the switching frequency.

10.3 Derive the expressions for Z_N and Z_D in Table 10.1.

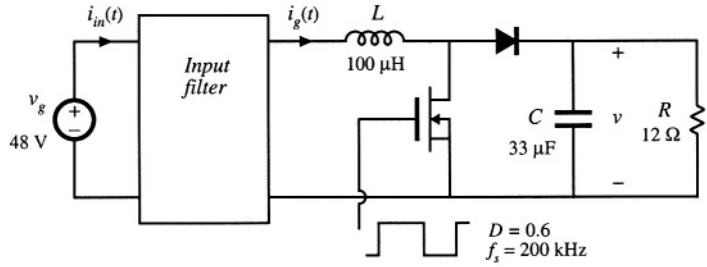

Fig. 10.31 Boost converter, Problems 10.2, 10.5, 10.7, and 10.9.

10.4 The input filter for the flyback converter of Fig. 10.30 is designed using a single L_f-C_f section. The filter is damped using a resistor R_f in series with a very large blocking capacitor C_b.

(a) Sketch a small-signal model of the flyback converter. Derive expressions for $Z_N(s)$ and $Z_D(s)$ using your model. Sketch the magnitude Bode plots of Z_N and Z_D, and label all salient features.

(b) Design the input filter, i.e., select the values of L_f, C_f, and R_f, so that: (*i*) the filter attenuation at the switching frequency is at least 100 dB, and (*ii*) the magnitude of the filter output impedance $Z_o(s)$ satisfies the conditions $\| Z_o(j\omega) \| < 0.3 \| Z_D(j\omega) \|$, $\| Z_o(j\omega) \| < 0.3 \| Z_N(j\omega) \|$, for all frequencies.

(c) Use Spice simulations to verify that the filter designed in part (b) meets the specifications.

(d) Using Spice simulations, plot the converter control-to-output magnitude and phase responses without the input filter, and with the filter designed in part (b). Comment on the changes introduced by the filter.

10.5 It is required to design the input filter for the boost converter of Fig. 10.31 using a single L_f-C_f section. The filter is damped using a resistor R_f in series with a very large blocking capacitor C_b.

(a) Sketch the magnitude Bode plots of $Z_N(s)$ and $Z_D(s)$ for the boost converter, and label all salient features.

(b) Design the input filter, i.e., select the values of L_f, C_f, and R_f, so that: (*i*) the filter attenuation at the switching frequency is at least 80 dB, and (*ii*) the magnitude of the filter output impedance $Z_o(s)$ satisfies the conditions $\| Z_o(j\omega) \| < 0.2 \| Z_D(j\omega) \|$, $\| Z_o(j\omega) \| < 0.2 \| Z_N(j\omega) \|$, for all frequencies.

(c) Use Spice simulations to verify that the filter designed in part (b) meets the specifications.

(d) Using Spice simulations, plot the converter control-to-output magnitude and phase responses without the input filter, and with the filter designed in part (b). Comment on the changes in the control-to-output responses introduced by the filter.

10.6 Repeat the filter design of Problem 10.4 using the optimum filter damping approach described in Section 10.4.1. Find the values of L_f, C_f, R_f, and C_b.

10.7 Repeat the filter design of Problem 10.5 using the optimum filter damping approach of Section 10.4.1. Find the values of L_f, C_f, R_f, and C_b.

10.6 Repeat the filter design of Problem 10.4 using the optimum R_f-L_b parallel damping approach described in Section 10.4.2. Find the values of L_f, C_f, R_f, and L_b.

10.9 Repeat the filter design of Problem 10.5 using the optimum R_f-L_b parallel damping approach described in Section 10.4.2. Find the values of L_f, C_f, R_f, and L_b.

10.10 It is required to design the input filter for the flyback converter of Fig. 10.30 using two filter sections. Each filter section is damped using a resistor in series with a blocking capacitor.

(a) Design the input filter, i.e., select values of all circuit parameters, so that (*i*) the filter attenuation at the switching frequency is at least 100 dB, and (*ii*) the magnitude of the filter output impedance $Z_o(s)$ satisfies the conditions $\| Z_o(j\omega) \| < 0.3 \| Z_D(j\omega) \|$, $\| Z_o(j\omega) \| < 0.3 \| Z_N(j\omega) \|$, for all frequencies.

(b) Use Spice simulations to verify that the filter designed in part (a) meets the specifications.

(c) Using Spice simulations, plot the converter control-to-output magnitude and phase responses without the input filter, and with the filter designed in part (b). Comment on the changes introduced by the filter.